Role of extended fins and graphene nano-platelets in coupled thermal enhancement of latent heat storage system

Zakir Khan [a,b], Zulfiqar Ahmad Khan [a*]

[a] Bournemouth University, Department of Design & Engineering, NanoCorr, Energy and Modelling (NCEM) Research Group, Fern Barrow, Talbot Campus, Poole, Dorset BH12 5BB, UK.

[b] School of Mechanical & Manufacturing Engineering (SMME), National University of Sciences & Technology (NUST), Sector H-12, Islamabad – 44000, Pakistan.

Corresponding Author:

[a*] Bournemouth University, Department of Design & Engineering, NanoCorr, Energy and Modelling (NCEM) Research Group, Fern Barrow, Talbot Campus, Poole, Dorset BH12 5BB, UK.

E-mail: zkhan@bournemouth.ac.uk

Tel.: +44 1202-961645

Abstract

To bring modernisation in low carbon economy, the latent heat storage (LHS) systems are crucial for sustainable future of smart energy generation and management systems for renewable sources. This article provides in–depth numerical analyses of 3-dimensional computational models incorporating coupled thermal enhancement techniques for identifying optimal solution to guarantee higher charging rate, higher total enthalpy and better thermal distribution of LHS system. Paraffin is selected as phase change material (PCM), graphene nano-platelets (GNP) as nano-additives and longitudinal, circular and wire-wound fins as extended surfaces in vertical shell-and-tube configurations. Based on numerical analyses, the extended surfaces have registered better thermal distributions and charging rates as compared to nano-PCMs. The geometrical orientation of extended surfaces and volume concentration of nano-additives have significant influence on melt front movement, natural convection and heat transfer performance. The peak values of heat fluxes are significantly increased from 2.25 kW/m^2 for paraffin without thermal enhancement to 35.86, 47.23 and 88.13 kW/m^2 for nano-PCM with 1% GNP in circular, longitudinal and wire-wound fins configurations. Hence, the charging duration for capturing 11.09 MJ is significantly reduced to mere 1.02 h for wire-wound fins configuration as compared to 23.5 h for paraffin without thermal enhancement. Likewise, the charging rate of wire-wound fins configuration is 20.95%, 35.96% and 89.94% higher than circular fins, longitudinal fins and nano-PCMs without extended surfaces, respectively. Moreover, the increase in volume concentration from 1% to 5% has adverse implications on accumulative enthalpy, natural convection and charging rate. Therefore, the novel design of coupled enhancement with wire-wound fins configuration and nano-PCM with 1% GNP are established as optimum solution for potential wide-ranging practical utilisations of LHS system.

Keywords

Thermal energy storage (TES); Latent heat storage (LHS); Graphene nano-platelets; Nano-PCM; Coupled thermal enhancement; Shell-and-tube heat exchanger

Nomenclature

C	mushy zone constant	μ	dynamic viscosity (kg/m.s)
C_p	specific heat capacity (kJ/kg.K)	Φ_{VC}	volume concentration of nano-particles
d	diameter (m)	β	thermal expansion coefficient (1/K)
f	liquid fraction	ρ	density (kg/m^3)
$\vec{\mathrm{g}}$	gravitational acceleration (m/s^2)	Subscripts	
H	total enthalpy (kJ)	L	liquefied phase
k	thermal conductivity (W/m.K)	S	solidified phase
k_B	Boltzmann constant	NP	nano-particles
L	latent heat capacity (kJ/kg)	PCM	base paraffin
M_W	molecular weight	$NPCM$	nano-PCM
N_A	Avogadro number	REF	reference
P	pressure (N/m^2)	Acronyms	
q	heat source term (W/m^3)	GNP	graphene nano-platelets
T	temperature (^{o}C)	HTF	heat transfer fluid
t	time (s)	LHS	latent heat storage
V	volume (m^3)	Nu	Nusselt number
$\vec{V}$	velocity (m/s)	PCM	phase change material
w	weight (kg)	VC	volume concentration

Greek

α	small constant value

1. Introduction

Fossil fuels have served the mankind for decades as primary energy sources. However, the continued increase in global economic growth and societal expansions seek provisions for additional energy. An over-reliance on fossil fuels to meet energy demands will pose serious threats to sustainable future due to their rapidly depleting resources, inconsistent prices and hazardous environmental implications. Technological developments for renewable sources are crucial to alleviate the dependency on fossil fuels and ensure energy security [1-3]. However, the intermittent characteristics of renewable sources are undesirable and detrimental to wide-ranging usefulness and effectiveness of renewable technologies. Energy storage systems are regarded as pivotal in augmenting the usability of renewable sources. Latent heat storage (LHS) systems are recognised as promising technologies due to their higher energy density, isothermal energy storage, phase change materials (PCM) availability

at wide range of temperatures, longer thermo-physical stability and lower vapour pressure [4, 5]. However, the main downsides are their unconvincing energy storage and retrieval rates due to poor thermal conductive nature of PCMs. In last decade, a significant body research is published on investigating thermal enhancement techniques to include: geometrical orientation with extended surfaces, dispersion of nano-additives, inclusion of metal matrices and encapsulations [6-8].

Shell-and-tube configurations are favoured due to their promising heat transfer performance and smoother integration to wider applications. In previous literature, the extended surfaces dimensions, types and numbers are extensively investigated for optimal thermal enhancement. Niyas et al. [9] conducted 3-dimensional numerical simulations on horizontal shell-and-tube with 0 – 6 longitudinal fins per tube. It was construed that the optimised configuration of 25 tubes with 4 – fins per tube can charge and discharge 16.94 MJ and 15.29 MJ in 2.28 h and 2.63 h, respectively. Joybari et al. [10] conducted 2-dimensional numerical analyses on charging/discharging rates of paraffin in horizontal tube-in-shell with longitudinal fins ranging from 0 – 8. It was reported that with an increase in fins number from 0 – 8, the charging/discharging durations were decreased by 54.67% and 85.48%, respectively. It was also reported that fins length and orientation are influential factors on heat transfer performance. Khan et al. [11] performed 2-dimensional numerical simulations to investigate the influence of number of tube passes, geometrical dimensions, positioning and construction materials of longitudinal fins on thermal storage capacity and phase transition rates in vertical shell-and-tube configuration. It was reported that conduction heat transfer improved with an increase in tube passes from 9 – 21. Likewise, the fins length was reported as more influential than the thickness, and the copper and aluminium as construction materials had demonstrated higher phase transition rates as compared to steel and cast iron. Furthermore, Khan and Khan. [12, 13] conducted experimental investigations on charging/discharging cycles of paraffin in the optimised novel design of shell-and-tube with 21 – tube passes and 76 – longitudinal fins. It was reported that the total enthalpy of 14.36 MJ and 12.09 MJ were charged/discharged in mere 3.12 h and 1.5 h, respectively. It was also reported that natural convection has significant impact on charging cycles and minimal influence on conduction dominant discharging cycles. Similar importance of natural convection influence on thermal distribution and phase transition rates are highlighted in [14, 15].

Lohrasbi et al. [16] performed 2-dimensional numerical optimisation procedure on phase transition rate and energy storage capacity of shell-and-tube with circular, longitudinal and v-shaped fins. It was reported that as compared to no-fins configuration, the extended surfaces improved thermal penetrations and resulted in 3.55, 3.26 and 4.28 times higher phase transition rates, respectively. Caron-Soupart et al. [17] reported that the longitudinal and circular fins reduced the thermal storage density from 49.2 kWh/m^3 for tube with no-fins to 46.5 kWh/m^3 and 45.9 kWh/m^3, respectively. In addition to longitudinal and circular fins, the other extended surfaces include helical and spiral fins [18, 19], branched and snowflake fins [20, 21], compact and plate fins [22, 23], and pin fins [24, 25]. In terms of design effectiveness, the type and orientations of extended surfaces in container are crucially influential for thermal reach and natural convection. Khan and Khan [26] reported that the charging effectiveness for vertical orientation of longitudinal fins was higher than horizontal orientation of longitudinal fins, compact fins and transversal squared fins. It can be construed

from literature that extended surfaces have significant potential for thermal enhancement, however it can simultaneously increase the overall weight of LHS system.

Inclusion of nano-additives, with their minimal increase in overall weight, is another thoroughly researched technique for thermal enhancement of LHS systems. Nano-additives are grouped into: i) metal nano-particles and ii) carbon allotropes. Said and Hassan [27] incorporated Cu, Al_2O_3 and CuO based nano-additives in paraffin with 1% and 5% volume concentrations to examine the thermal enhancement in rectangular heat exchanger coupled with air-conditioning system. It was reported that the coefficient of performance and power saving of the air-conditioning system improved with dispersion of nano-particles. Cu based nano-PCM illustrated higher power saving of 7.41% as compared to 7.28% and 7.35% by Al_2O_3 and CuO based nano-PCMs. Ebadi et al. [28] reported that inclusion of higher concentration of CuO would not guarantee proportional enhancement in charging rates. Golestaneh et al. [29] reported that the inclusion of even small weight concentration of Al_2O_3, Fe_2O_3, SiO_2 and ZnO based nano-particles had significantly reduced the total enthalpy of nano-PCMs.

Khan and Khan [30] conducted numerical and experimental investigations on Al_2O_3, AlN and GNP nano-additives with paraffin in shell-and-tube configuration. It was reported that as compared to base paraffin, the charging rates were augmented by 28.01%, 36.47% and 44.57%, and the discharging rates were improved by 14.63%, 34.95% and 41.46%, respectively. It was also reported that with an increase in volume concentrations from 1% – 5%, the overall enthalpy reduced from 4.75% – 20.58%, 4.46% – 19.64% and 0.55% – 2.88%, as compared to base paraffin. Hence, the GNP based nano-PCMs were recommended due to their higher thermal enhancement and minimal reduction in overall enthalpy. Warzoha and Fleische [31] evaluated the charging/discharging performance enhancement of paraffin by incorporating Al, TiO_2, MWCNT and GNP nano-particles with 20 vol.%. It was reported that the total melting and solidification duration was significantly reduced from 1.9 h for base paraffin to 1.58 h, 1.67 h, 1.38 h and 1.33 h for respective nano-PCM. Tang et al. [32] synthesised and evaluated the Al_2O_3 and GNP based nano-PCMs. It was reported that with an increase in weight concentration from 4% – 12%, the respective thermal conductivity was significantly augmented from 0.28 – 0.39 W/m.K and 0.32 – 0.45 W/m.K, as compared to 0.20 W/m.K for base material (MA/HDPE). It was noticed that thermal enhancement would not respond linearly to increasing volume concentration of nano-additives. Yuan et al. [33] reported that the latent enthalpy reduced from 166.5 – 140.53 kJ/kg and 167.47 – 132.95 kJ/kg for GNP and EG based nano-PCMs as the weight concentrations increased from 1% – 8%, respectively. Yu et al. [34] evaluated the thermal enhancement in paraffin with inclusion of carbon allotropes including: MWCNT, CNF and GNP. It was reported that GNP based nano-PCM had outperformed other allotropes by demonstrating significantly higher thermal conductivity and relatively moderate increase in dynamic viscosity. It can be deduced from literature that carbon allotropes have demonstrated higher potential for thermal enhancement as compared to metal nano-particles. In addition, the smaller density of carbon allotropes ensures longer thermo-physical stability, excellent dispersion and insignificant sedimentation and agglomeration issues, which are common downsides of metal nano-particles. Moreover, the identification of optimal concentration of carbon allotropes are crucial due to simultaneous escalation in dynamic viscosity which bears adverse impacts on natural convection and thermal distribution.

In order to complement the advantages and diminish the downsides of extended surfaces and nano-additives, the coupled enhancement techniques have higher potentials for further upgrading the thermo-physical performance. Mahdi et al. [35] reported that solidification duration of paraffin in horizontal shell-and-tube with longitudinal fins and Al_2O_3 nano-additives was reduced by 30.2% as compared to 1.8% reduction by Al_2O_3 without longitudinal fins. Singh et al. [36, 37] reported that the charging and discharging rates of d-mannitol were augmented from 47% – 68% and 26% – 49% with inclusion of 5 vol.% of GNP in vertical shell-and-tube with circular fins configuration. Sheikholeslami et al. [38] conducted numerical analyses on coupled enhancement with longitudinal fins and CuO nano-particles. It was reported that the discharging rate for coupled enhancement scenario was higher as compared to fins without nano-additives. On the contrary, Parsazadeh and Duan [39] reported that the inclusion of 4 vol.% of Al_2O_3 with longitudinal fins in vertical shell-and-tube had produced rather weaker charging rate as compared to longitudinal fins without Al_2O_3.

It is deduced that the literature lacks a) the design and analyses of novel geometrical configuration of extended surfaces which could develop on the strengths of longitudinal and circular fins and reduce their limitations, b) the detailed transient numerical analyses of novel geometrical configuration in 3-dimensional rather than 2-dimensional computational domain, c) the comprehensive thermo-physical performance evaluations of nano-PCMs in novel designed shell-and-tube rather than merely focusing on the synthesis, and d) the comparative analyses of coupled enhancement techniques with varied extended surfaces and nano-PCMs with varied volume concentrations. This article is focused on addressing the above-mentioned literature gaps by conducting transient numerical simulations on 3-dimensional computational domains of shell-and-tube with varied extended surfaces and nano-additives with varied volume concentrations. The novel design configuration of shell-and-tube with wire-wound fins is proposed and evaluated with and without nano-additives, which is neither considered in our previous publications nor reported elsewhere in literature. The coupled thermal enhancement with varied extended surfaces and nano-additives contribute to fourteen scenarios. Numerical analyses help in thermo-physical evaluations of these scenarios through phase transition rates, overall enthalpy accumulation, temperature distribution, melt front propagation and heat transfer characterisation, which is unprecedented.

2. Numerical Model

2.1. Physical model and computational domains

This article is focused to provide an optimal design solution for an efficient and responsive LHS system comprising novel geometrical orientations of extended surfaces in shell-and-tube heat exchanger and nano-additives enhanced thermal storage material. The geometrical configuration of multi-tube passes in shell container along with varied extended surfaces such as longitudinal, circular and wire-wound fins are illustrated in **Fig. 1**. The purpose of conducting 3-dimensional numerical investigations on varied extended surfaces configurations are to identify a novel design solution which can guarantee better temperature distribution, higher heat transfer performance, higher charging rates and maintain higher total enthalpy.

The vertical shell container is made of copper with outer diameter and thickness of 450 mm and 1 mm, respectively. It can be noticed that each geometrical configuration consists of seven tube passes with extended surfaces in shell container which enables the formation of symmetrical computational domains, as shown in **Fig. 1**. In order to conduct comparative analyses, the thickness, length and volume occupied by extended surfaces in computational domains are constrained to 1 mm, 50.8 mm and 93.5 ml, respectively. The tube and extended surfaces are made of copper. Paraffin (RT44HC) is selected as PCM due to its higher latent heat capacity, good thermo-physical reliability and excellent compatibility with metals [5]. Graphene nano-platelets are chosen as nano-additives due to their higher thermal conductivity, lower density and desirable long-term suspension behaviour in base paraffin [30]. Thermo-physical characteristics of paraffin, copper and graphene are listed in **Table 1**. Moreover, water is utilised as heat transfer fluid (HTF) to circulate in multi-tube passes and charge nano-PCM in shell container.

Table 2 provides the list of coupled thermal performance enhancement cases including tube configurations with and without extended surfaces, paraffin with and without nano-additives and their respective packing factors. Therefore, this article provides comprehensive thermal performance evaluations by conducting transient numerical investigations on charging cycles of all fourteen cases.

Table 1
Thermo-physical characteristics of base paraffin, copper and graphene [40, 41]

	Paraffin (RT44HC)	Copper	Graphene
Density (kg/m^3)	800 (s), 700 (l)	8920	400
Thermal conductivity (W/m.K)	0.2	400	3000
Specific heat capacity (J/kg.K)	2000	380	643
Latent heat capacity (J/kg)	255000	-	-
Phase transition temperature (^{o}C)	41-44	-	-

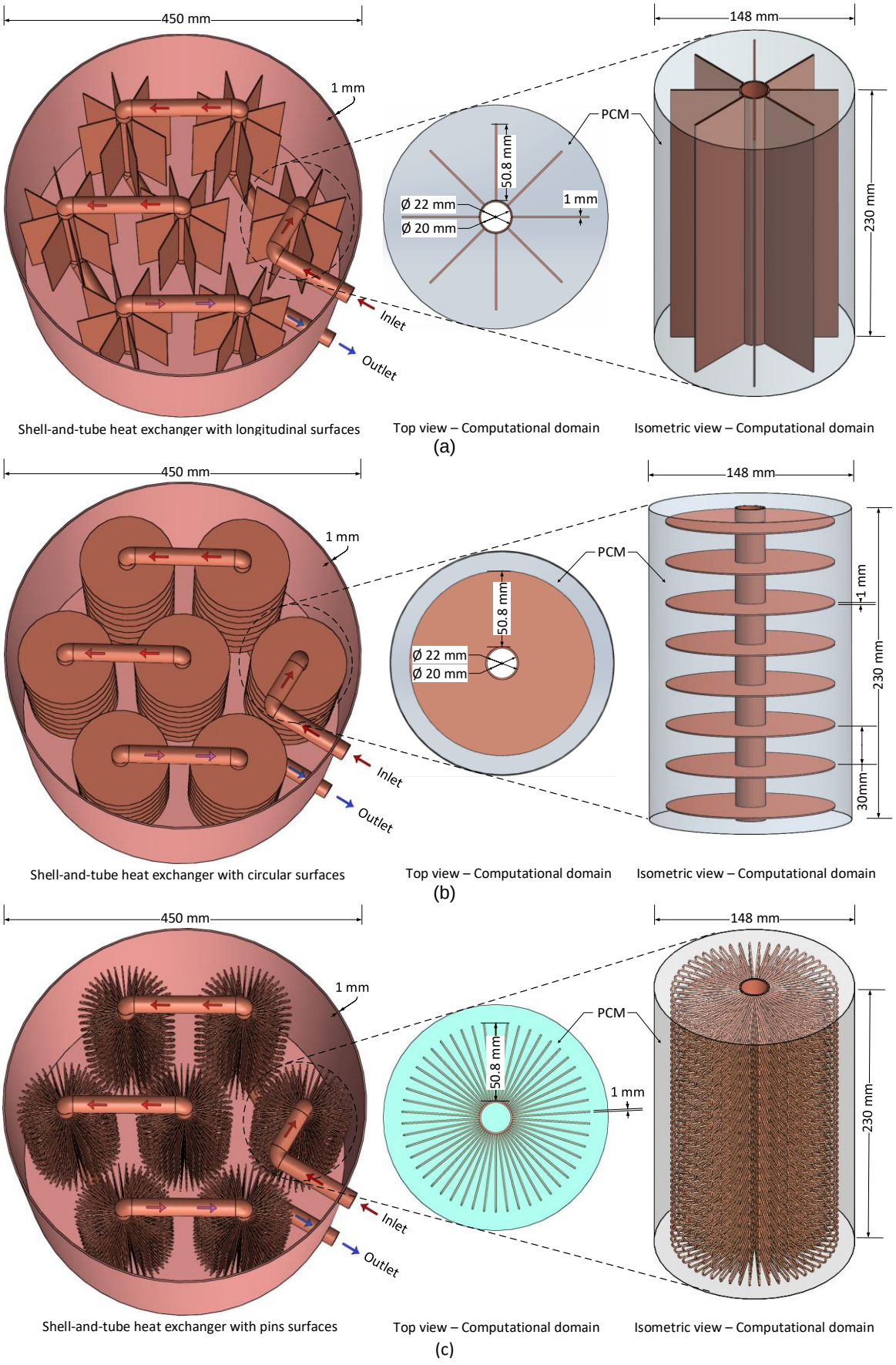

193 **Fig. 1** Shell-and-tube heat exchanger with multi-tube passes and varied extended surfaces
194 orientations: (a) longitudinal fins, (b) circular fins and (c) wire-wound fins.

Table 2
List of coupled thermal performance enhancement cases and their respective packing factor

Case No.	Tube configuration	Thermal storage material					Packing factor $\varphi_{P.F} = \frac{V_{PCM}}{V_S}$
		Paraffin	Nano-PCM				
			1% VC	2.5% VC	3% VC	5% VC	
1	Plain (no-fins)	✓					1
2	Plain (no-fins)			✓			0.975
3	Longitudinal fins	✓					0.975
4	Longitudinal fins		✓				0.965
5	Longitudinal fins				✓		0.945
6	Longitudinal fins					✓	0.925
7	Circular fins	✓					0.975
8	Circular fins		✓				0.965
9	Circular fins				✓		0.945
10	Circular fins					✓	0.925
11	Wire-wound fins	✓					0.975
12	Wire-wound fins		✓				0.965
13	Wire-wound fins				✓		0.945
14	Wire-wound fins					✓	0.925

2.2. Governing equations

The following assumptions are considered to reduce the computational complexity of 3-dimensional transient numerical simulations of coupled thermal performance enhancement cases:

a) Due to geometrical symmetry of computational domains in shell container, the heat transfer from outer boundary of computational domains are neglected.
b) Temperature variations of HTF in computational domain are negligible and hence, constant inlet wall temperature is assigned for all charging cycles.
c) The volumetric expansion and shrinkage of nano-PCM associated with phase change are neglected.
d) Boussineq approximation is valid for computing buoyancy driven natural convection.

A numerical model is developed by considering the above assumptions and the governing equations for mass, momentum and energy conservations, as given below:

Mass conservation:

$$\frac{\partial \rho}{\partial t} + \nabla.\left(\rho \vec{V}\right) = 0 \tag{1}$$

Momentum conservation:

$$\frac{\partial\left(\rho \vec{V}\right)}{\partial t} + \rho \vec{V}.\left(\nabla.\vec{V}\right) = -\nabla P + \mu \nabla^2.\vec{V} + \rho\beta\vec{g}(T - T_{REF}) + \frac{C(1-f)^2}{(f^3+\alpha)}\vec{V} \tag{2}$$

Energy conservation:

$$\frac{\partial(\rho H)}{\partial t} + \nabla.\left(\rho H.\vec{V}\right) = \nabla.\left(\frac{k}{\rho C_P}\nabla H\right) + q \tag{3}$$

In order to model the phase transition between solid–mushy–liquid, the enthalpy–porosity technique is implemented. Boussineq approximation is included in momentum conservation equation to account for buoyancy driven upward movement of lower density molecules with respect to increasing temperature [42]. Due to transient variations in the density of nano-

PCM with temperature, the instantaneous natural convection response to melting process is of significant importance. Moreover, the momentum sink term account for mushy zone porosity, which is derived from Darcy law for porous medium [43]. The phase transition between solid–mushy–liquid cause variations in the velocity of nano-PCM. Therefore, a morphological constant C is introduced to control the damping effects in mushy zone, with desirable value ranging from $10^5 - 10^6$. In this article, the numerical simulation of nano-PCMs with $C = 10^6$ have produced matching results with experimental results in [30]. Similarly, α is a small computational constant ($\alpha = 10^{-3}$) which is employed to avoid division by zero. During phase transition, the liquid fraction f ranges between 0 (solid) – 1 (liquid) and is defined as the function of temperature:

$$f = \begin{cases} 0 & T < T_S \\ \dfrac{T - T_S}{T_L - T_S} & T_S \leq T \leq T_L \\ 1 & T > T_L \end{cases} \tag{4}$$

In energy conservation equation, the total enthalpy is the summation of reference enthalpy, sensible enthalpy and latent enthalpy, as follow:

$$H = h_{REF} + \int_{T_{REF}}^{T} C_P dT + fL \tag{5}$$

The coupled thermal performance enhancement involve both extended surfaces and nano-additives enhanced paraffin or nano-PCM. **Table 1** provides thermo-physical characteristics of paraffin as base material and graphene as nano-additives. In order to estimate the variations in thermo-physical characteristics of nano-PCM, the following relations for mixture of two components are implemented [44]:

$$\rho_{NPCM} = (1 - \Phi_{VC})\rho_{PCM} + \Phi_{VC}\rho_{NP} \tag{6}$$

$$L_{NPCM} = \frac{(1 - \Phi_{VC})\rho_{PCM} L_{PCM}}{\rho_{NPCM}} \tag{7}$$

$$C_{P,NPCM} = \frac{(1 - \Phi_{VC})\rho_{PCM} C_{P,PCM} + \Phi_{VC}\rho_{NP} C_{P,NP}}{\rho_{NPCM}} \tag{8}$$

$$\beta_{NPCM} = \frac{(1 - \Phi_{VC})\rho_{PCM}\beta_{PCM} + \Phi_{VC}\rho_{NP}\beta_{NP}}{\rho_{NPCM}} \tag{9}$$

Moreover, the transient variations in dynamic viscosity of nano-PCM with respect to operating temperature, volume concentration and particle size of nano-additives are evaluated by employing the semi-empirical correlation proposed by Corcione [45], as given below:

$$\mu_{NPCM} = \frac{\mu_{PCM}}{1 - 34.87(d_{NP}/d_{PCM})^{-0.3}{\Phi_{VC}}^{1.03}} \tag{10}$$

where d_{NP} represents the diameter of graphene nano-platelets, which is equal to 6 nm [30, 41]. Similarly, the equivalent diameter d_{PCM} and dynamic viscosity μ_{PCM} of base paraffin are determined from following relations [45, 46]:

$$d_{PCM} = 0.1\left(\frac{6M_W}{\pi N_A \rho_{PCM,O}}\right)^{0.333} \tag{11}$$

$$\mu_{PCM} = 0.001exp\left(-4.25 + \frac{1790}{T}\right) \tag{12}$$

Moreover, the transient modifications in effective thermal conductivity of nano-PCM with respect to operating temperature, volume concentration and particle size of graphene nano-platelets are determined by implementing the empirical correlations proposed by Vajjha and Das [47], as follow:

$$k_{NPCM} = \frac{k_{NP} + 2k_{PCM} - 2(k_{PCM} - k_{NP})\Phi_{VC}}{k_{NP} + 2k_{PCM} + (k_{PCM} - k_{NP})\Phi_{VC}} k_{PCM} + 5 \times 10^4 \zeta \rho_{PCM} \Phi_{VC} C_{P,PCM} \sqrt{\frac{\kappa_B T}{\rho_{NP} d_{NP}}} f(T, \Phi_{VC}) \tag{13}$$

$$f(T, \Phi_{VC}) = (2.8217 \times 10^{-2}\Phi_{VC} + 3.917 \times 10^{-3})\left(\frac{T_{NPCM}}{T_{REF}}\right) + (-3.0669 \times 10^{-2}\Phi_{VC} - 3.91123 \times 10^{-3}) \tag{14}$$

where $f(T, \Phi_{VC})$ is the correction factor, which accounts for Brownian motion of graphene nano-platelets in liquid paraffin. Thermo-physical characteristics of nano-PCMs with varied volume concentrations of 1%, 3% and 5% are derived from Eq. (6) – Eq. (14), as shown in **Table 3**.

Table 3
Thermo-physical properties of nano-PCM with varied volume concentration in solid and liquid phases

	Nano-PCM					
	1% VC		3% VC		5% VC	
	Solid	Liquid	Solid	Liquid	Solid	Liquid
Density (kg/m^3)	796.00	697.00	788.00	691.00	780.00	685.00
Specific heat capacity (J/kg. K)	1993.18	1992.21	1979.34	1976.43	1965.21	1960.38
Latent heat capacity (J/kg)	253.72×10^3	253.54×10^3	251.12×10^3	250.57×10^3	248.46×10^3	247.55×10^3
Thermal expansion coefficient (1/K)	298.61×10^{-6}	298.41×10^{-6}	295.79×10^{-6}	295.20×10^{-6}	292.91×10^{-6}	291.93×10^{-6}
Dynamic viscosity (kg/m.s)	7.04×10^{-3}	2.89×10^{-3}	8.91×10^{-3}	3.66×10^{-3}	12.2×10^{-3}	5.02×10^{-3}
Thermal conductivity (W/m.K)	0.276	0.484	0.281	0.498	0.291	0.523

* Solid and liquid represent thermo-properties of nano-PCM at 20 ^{o}C and 70 ^{o}C, respectively.

2.3. Initial and boundary conditions

During charging cycle, the heat transfer occurs between high temperature water circulating in multi-tube passes and low temperature nano-PCM in shell container. As the charging cycle progresses, the nano-PCM accumulates thermal energy and consequently, it undergoes phase transition from solid–mushy–liquid. To simulate the charging cycle, the volume of nano-PCM in computational domain (see **Fig. 1**) is set to an initial temperature of 10 ^{o}C which assures the initial solid state. Likewise, the inside face of tube in computational domain is set to constant inlet temperature of 62 ^{o}C, which mimics the high temperature

water from solar collector [13]. The charging cycle concludes once the entire mass of nano-PCM undergoes phase transition to liquid state.

2.4. Numerical simulation technique

Finite volume method is adopted to discretise the governing equations for nano-PCMs in 3–dimensional computational domains shown in **Fig. 1**. The transient charging cycles are solved using sequential pressure–based solution algorithm. To achieve the pressure–velocity coupling in momentum conservation equation (Eq. 2), the higher order pressure–implicit with splitting of operators (PISO) algorithm is employed. The spatial discretisation of gradients and derivatives are obtained from Green-Gauss node based method. Pressure staggering option (PRESTO) scheme is employed for natural convection. Moreover, the second order upwind scheme is implemented for spatial discretisation of convective terms in momentum and energy conservation equations. The solution controls with under-relaxation factors for pressure, momentum and energy are set to 0.3, 0.7 and 1, respectively [48]. The convergence conditions for continuity, velocity and energy equations are monitored with residual criteria programmed at 10^{-6}, respectively. Furthermore, the stable computational solutions for transient charging cycles are achieved by implementing first order implicit formulation with fixed time stepping iterative advancement approach.

2.5. Time step and grid independency tests

The precision and reliability of numerical simulations for various computational domains are established by investigating time step and grid resolution independencies. Three varied time steps of 0.1, 0.5 and 1 s and three grid resolutions with maximum element size of 0.5, 0.75 and 1 mm for all computational domains including tube with no-fins, longitudinal fins, circular fins and wire-wound fins configurations are simulated. **Table 4** provides the liquid fraction of paraffin subjected to charging cycle for 1 h for all abovementioned scenarios and the percent errors are also computed. In case of grid independency tests, the time step of 1 s is selected for simulation. The grid resolution independency for all scenarios are established with mesh sizes of 5.35×10^{7}, 3.70×10^{7}, 2.35×10^{7} and 8.08×10^{7}, respectively. Similarly, in case of time step independency, the established mesh sizes are simulated with varied time steps. It is evident that the liquid fraction for all scenarios are almost identical with percent error ranging between 0.01% – 0.57%. Therefore, the time step of 1 s is selected to help reduce the computational cost.

2.6. Experimental validation

In order to establish the accuracy and robustness of numerical simulations, the transient temperature results are compared with the experimental results for paraffin in longitudinal fins orientation [13] and nano-PCM in shell-and-tube heat exchanger [30], as presented in **Fig. 2**. In both cases, the numerical simulations are performed for computational domains by taking into consideration the geometrical configurations and dimensions, initial and boundary conditions and material properties as reported in [13, 30]. It is evident that the numerical and experimental temperature curves are in good agreement. The mean absolute percentage errors for paraffin in longitudinal fins orientation and nano-PCM in shell-and-tube heat exchanger are 2.35% and 2.67%, respectively.

Table 4
Time step and grid resolution independency tests for computational domain of tube with no-fins, longitudinal fins, circular fins and wire-wound fins.

Tube configuration	Max element size (mm)	Mesh size	Liquid fraction after 1 hr	Percent error	Time steps	Liquid fraction after 1 hr	Percent error
Plain tube (no-fins)	1	$4.19x10^6$	0.1351	10.20	0.1 s	0.1219	0.57
	0.75	$9.09x10^6$	0.1243	1.39	0.5 s	0.1224	0.16
	0.5	**$5.35x10^7$**	**0.1226**	**-**	**1 s**	**0.1226**	**-**
Tube with longitudinal fins	1	$4.10x10^6$	0.7678	4.75	0.1 s	0.7326	0.05
	0.75	$9.60x10^6$	0.7433	1.41	0.5 s	0.7329	0.01
	0.5	**$3.70x10^7$**	**0.7330**	**-**	**1 s**	**0.7330**	**-**
Tube with circular fins	1	$3.76x10^6$	0.9122	4.08	0.1 s	0.8755	0.10
	0.75	$8.15x10^6$	0.8856	1.05	0.5 s	0.8757	0.08
	0.5	**$2.35x10^7$**	**0.8764**	**-**	**1 s**	**0.8764**	**-**
Tube with Wire-wound fins	1	$3.55x10^7$	0.9823	1.22	0.1 s	0.9695	0.10
	0.75	**$8.08x10^7$**	**0.9705**	-	0.5 s	0.9698	0.07
	0.5	$2.73x10^8$	0.9700	0.05	**1 s**	**0.9705**	**-**

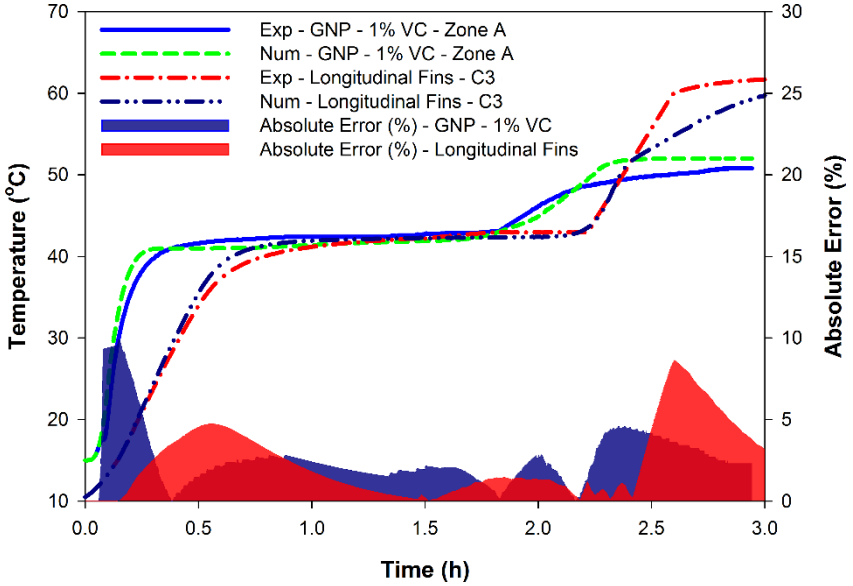

Fig. 2 Numerical model validations with experimental results for paraffin in longitudinal fins and nano-PCM in shell-and-tube heat exchanger.

3. Results and Discussion

In order to evaluate the couple thermal performance enhancement cases listed in **Table 2**, the charging cycle of paraffin in plain tube orientation (case 1) is selected as standard for comparison. Likewise, the influence of various geometrical configurations with nano-PCMs on charging cycles are analysed from transient variations in temperature, liquid fraction, total enthalpy, heat flux and heat transfer coefficient, velocity and Nusselt number (Nu).

In case of charging cycles, the temperature gradient between water in tube and nano-PCM in shell container actuates heat transfer. In initial stages, the heat transfer rate is higher and the sensible enthalpy is rapidly captured by nano-PCM. In consequence, the temperature of nano-PCM increases until the phase transition temperature is reached (10 ^oC – 41 ^oC). At this point, the sensible energy storage capacity of nano-PCM is achieved. In next stages, the heat transfer rate reduces to certain level and is followed by gradual decline while capturing the latent enthalpy at almost isothermal temperature (41 ^oC – 44 ^oC). In the course of latent

enthalpy storage, the phase transition from solid–mushy–liquid shapes up. Upon completion of latent heat capacity, the liquid nano-PCM undergoes rapid increase in temperature until it reaches the inlet temperature of water. In these final stages, the sensible enthalpy of nano-PCM in liquid phase is stored as the temperature increases from 44 ^{o}C – 62 ^{o}C.

The impact of various geometrical configurations with and without nano-additives on thermal performance of LHS system are illustrated and discussed in the following sections.

3.1. Plain tube configuration – Case 1

In case 1, the thermal storage material is paraffin without graphene nano-platelets and geometrical configuration is comprised of tube without extended surfaces. **Fig. 3** illustrates the temperature, liquid fraction and enthalpy contours at various time intervals during the course of charging cycle. In **Fig. 3**, the top row represents the temperature contours in entire computational domain and the bottom row illustrates the cross-section of computational domain with temperature contours on the left side and liquid fraction and enthalpy on the right side. Likewise, **Fig. 4** illustrates the transient behaviour of paraffin by including the temperature, liquid fraction, velocity, total enthalpy, heat flux, heat transfer coefficient and Nu plots.

It can be observed that during initial stages, the higher temperature gradient results in rapid escalation of heat flux to its peak value of 2.257 kW/m^2. In these earlier stages, conduction is the dominant mode of heat transfer. Temperature contours illustrates that temperature of paraffin in close proximity to the heated wall of tube is increased. However, the regions at slight distance are still at low energy state which can depict the poor thermal propagation in low thermal conductive solid paraffins. Due to higher heat flux between heated wall of tube and the adjacent paraffin, the sensible and latent portions of enthalpy are rapidly absorbed and therefore, it experiences phase transition from solid–mushy–liquid. With an increase in liquid paraffin around the heated wall of tube, the buoyancy driven natural convection causes the upward rise of higher temperature and lower density liquid paraffin. Mean velocity and Nu of liquid paraffin surge to their peak values of 0.247 mm/s and 5.947, respectively. In next stages, the accumulation of higher temperature liquid paraffin in upper region of shell container increases and results in higher charging rate as compared to lower region. Heat flux remains steady with linear increase in enthalpy curve. As these stages progress, the natural convection intensifies, which results in further accumulation of liquid paraffin in top region. In final stages, the congestion and weaker mobility of liquid paraffin in top region result in linear and gradual decline in heat flux and mean velocity. Due to which, the liquid fraction, enthalpy and mean temperature curves illustrate a slower and logarithmic growth. Hence, the total charging time required for paraffin in case 1 is 26 h.

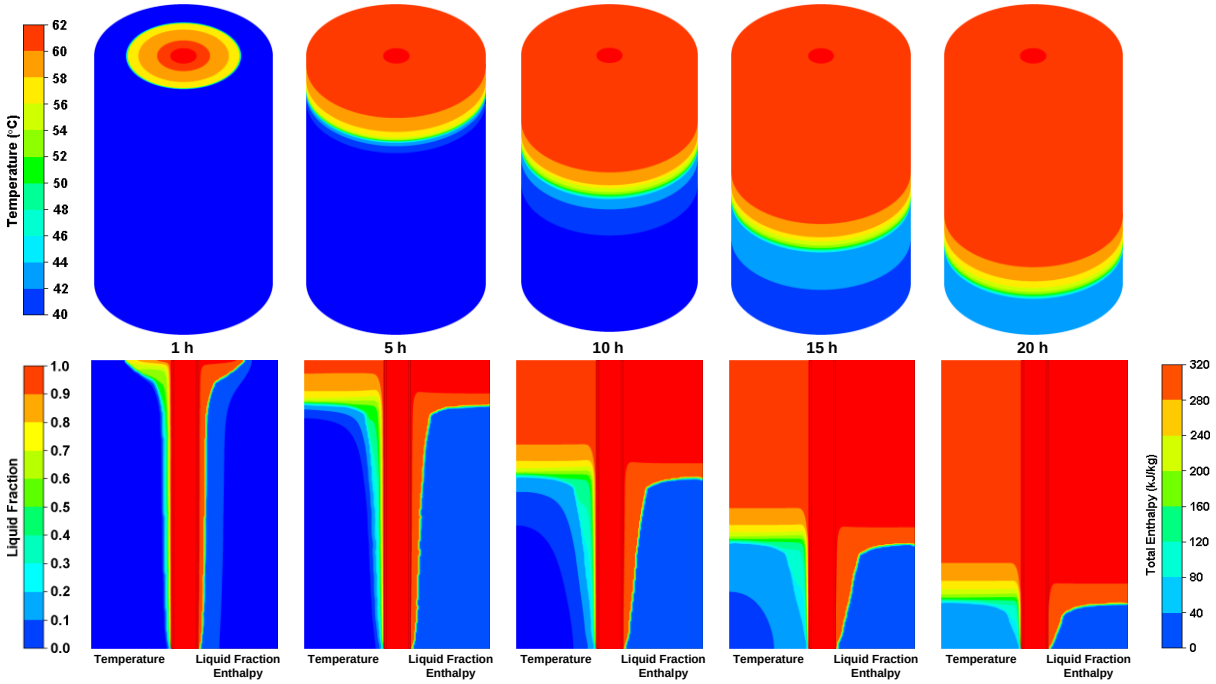

Fig. 3 Temperature, liquid fraction and enthalpy contours of paraffin in shell-and-tube without extended surfaces orientation while charging at constant inlet temperature of 62 °C.

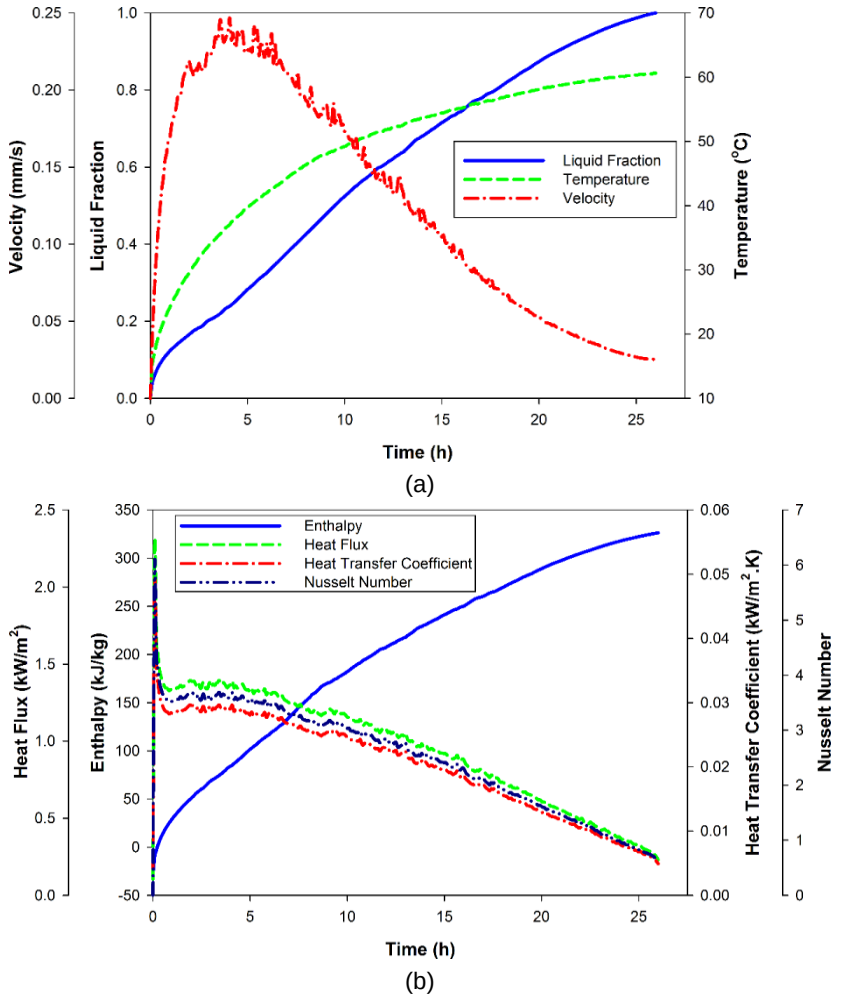

Fig. 4 Transient behaviour of paraffin during the course of charging cycle in shell-and-tube without extended surfaces.

3.2. Plain tube with nano-PCM configuration – Case 2

In case 2, the thermal storage material is nano-PCM with 2.5% volume concentration of graphene nano-platelets, as shown in **Table 2**. The packing factor of case 2 is 0.975, which is similar to case 3, 7 and 11. Hence, it ensures better comparisons between various thermal performance enhancement techniques. **Fig. 5 (a)** illustrates the temperature, liquid fraction and enthalpy contours and **Fig. 6 (a) and (b)** represent the transient responses to charging cycle.

The inclusion of high thermal conductive graphene nano-platelets supplements the effective thermal conductivity and surface area for heat transfer. It is evident from temperature and enthalpy contours that thermal propagation in case 2 is relatively improved as compared to case 1. Due to augmented effective thermal conductivity, the heat flux of nano-PCM reaches its peak value of 3.184 kW/m^2. In addition, the natural convection is slightly improved with peak value for mean velocity reaches to 0.259 mm/s. The reasons for slight enhancement in natural convection is that with inclusion of graphene nano-platelets, the effective dynamic viscosity also increases which curtails the buoyancy driven upward movement of nano-PCM. Despite that, the enhancements in temperature propagations and rates of enthalpy capture and phase transition are significant. For instance, the total charging time required for case 2 is 13.75 h, which is reduced by 47.12% as compared to case 1.

3.3. Longitudinal fins configuration – Case 3

In case 3, the computational domain comprises of paraffin as thermal storage material and tube with longitudinal fins as geometrical configuration for heat transfer. For similar packing factor, the thermal performance enhancement induced by graphene nano-platelets in case 2 and longitudinal fins in case 3 can be compared. During charging cycle, the thermal contours of paraffin in longitudinal fins configuration are illustrated in **Fig. 5 (b)** and the transient variations in **Fig. 6 (c) and (d)**, respectively.

As demonstrated in **Fig. 5 (b)**, the inclusion of longitudinal fins significantly enhances the radial thermal distribution and extends the thermal reach towards the shell boundary. The surface area for heat transfer is augmented by longitudinal fins and therefore, the peak heat flux of 39 kW/m^2 is generated. Hence, the accumulative enthalpy capture and phase transition rate for paraffin in regions closer to heated walls of tube with longitudinal fins are boosted. Moreover, the longitudinal fins orientation in computational domain promotes the buoyancy driven upward movement of higher temperature liquid paraffin. Due to higher natural convection, the peak values for mean velocity and Nu are escalated to 1.13 mm/s and 131.8, respectively. Therefore, the total charging time for paraffin in longitudinal fins orientation is shortened to 2.16 h. In other words, the charging rate is significantly improved by 91.67% and 84.24% as compared to case 1 and case 2, respectively.

3.4. Circular fins configuration – Case 7

In this case, the thermal performance enhancement of paraffin in circular fins configuration are evaluated by conducting the charging cycle at constant inlet temperature. **Fig. 5 (c)** illustrates the thermal contours and **Fig. 6 (d)** and **(e)** represent the transient responses of paraffin to charging cycle in circular fins configuration.

It can be noticed from temperature contours that the radial and vertical thermal distributions are significantly improved with inclusion of circular fins as compared to case 1–3. Although the length and thickness constraints of extended surfaces are applied, the thermal energy propagation towards the distant regions closer to shell boundary is apparently better than longitudinal fins. Hence, at earlier stages, the conduction dominant heat transfer enables the rapid capturing of thermal enthalpy. However, in next stages, the buoyancy driven natural convection is weakened by circular fins as it obstructs the upward movement of liquid paraffin. As a result, the peak values for heat flux, mean velocity and Nu merely reach to 31.11 kW/m^2, 0.842 mm/s and 39.32, respectively. Therefore, it can be deduced that conduction is the dominant mode of heat transfer in circular fins configuration. Whereas, the natural convection is significantly weaker as compared to longitudinal fins configuration. Despite the weaker natural convection, the total charging time required for paraffin in circular fins configuration is reduced to 1.75 h. Hence, the charging rate is significantly enhanced by 93.27%, 87.27% and 18.98% as compared to case 1–3, respectively.

3.5. Wire-wound fins configuration – Case 11

Thermal performance enhancement of paraffin in tube with wire-wound fins configuration are evaluated by numerical simulation of charging cycle. This novel geometrical configuration of tube with wire-wound fins is formulated to counter the limitations incurred in longitudinal and circular fins configurations. The length, thickness and occupied volume of wire-wound fins configuration conform to the specified constraints. Hence, it results in similar packing factor as compared to case 2, 3 and 7, as shown in **Table 2**. However, even for similar packing factor, the wire-wound fins configuration has generated significantly higher effective heat transfer area. For instance, the effective surface area for wire-wound fins is 85.05% and 83.57% higher as compared to longitudinal and circular fins configurations. Thermal contours and transient responses to charging cycle are illustrated in **Fig. 5 (d)** and **Fig. 6 (g)** and **(h)**, respectively.

Temperature contours demonstrate that the wire-wound configuration has relatively better radial and vertical thermal distribution as compared to tube without fins, with longitudinal fins and circular fins. The reason behind is the higher effective heat transfer area and the proximity of wire-wound fins to paraffin in both radial and vertical directions. As a result, the peak heat flux reaches to 82.93 kW/m^2 which is significantly higher as compared to earlier cases. Moreover, this novel compact design of wire-wound fins supports and strengthens the buoyancy driven natural convection. Due to which, the peak values for mean velocity and Nu are escalated to 1.427 mm/s and 197.2, respectively. Furthermore, the mean temperature, enthalpy capture and liquid fraction curves illustrate a steeper increase, which is followed by a gradual logarithmic increase in later stages of the charging cycle. It is construed that both conduction and natural convection are dominant modes of heat transfer in wire-wound fins configuration. Hence, the total charging time is lessened to mere 1.38 h. In other words, the charging rate for wire-wound fins configuration is 94.68%, 89.94%, 35.96% and 20.95% higher as compared to tube without fins, graphene nano-platelets enhanced paraffin in tube without fins, longitudinal fins and circular fins configurations, respectively.

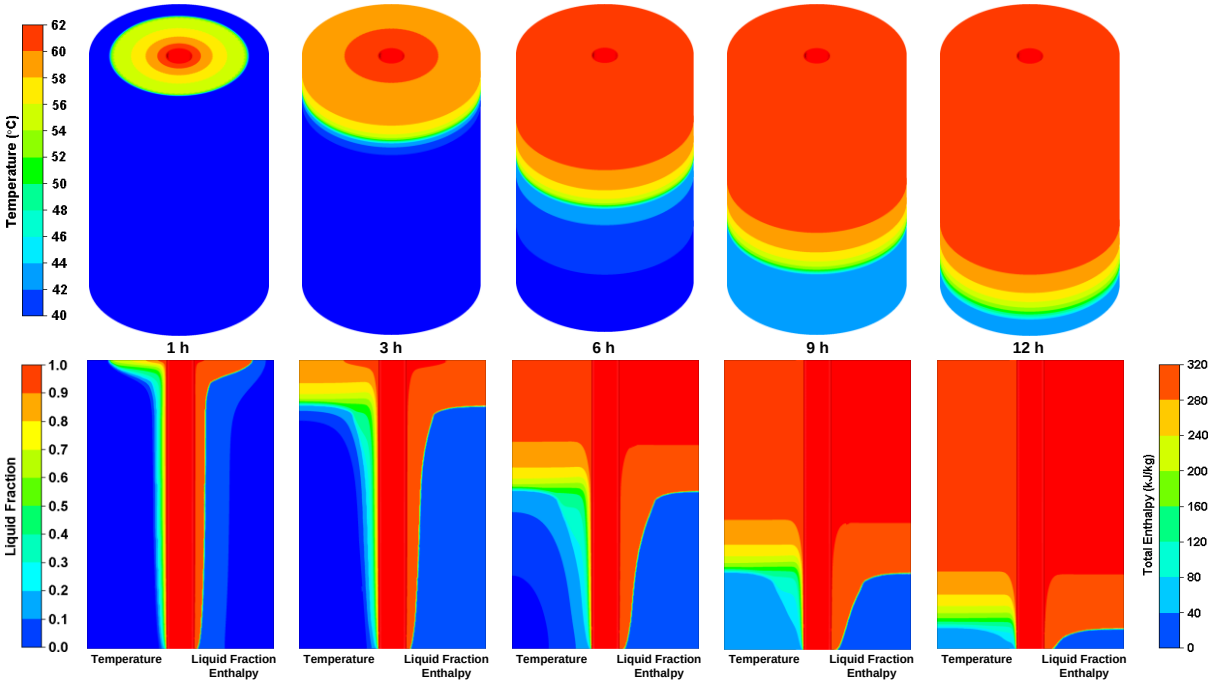
Temperature (°C)
62
60
58
56
54
52
50
48
46
44
42
40
1 h
3 h
6 h
9 h
12 h
Liquid Fraction
1.0
0.9
0.8
0.7
0.6
0.5
0.4
0.3
0.2
0.1
0.0
Temperature
Liquid Fraction
Enthalpy
Total Enthalpy (kJ/kg)
320
280
240
200
160
120
80
40
0

(a)

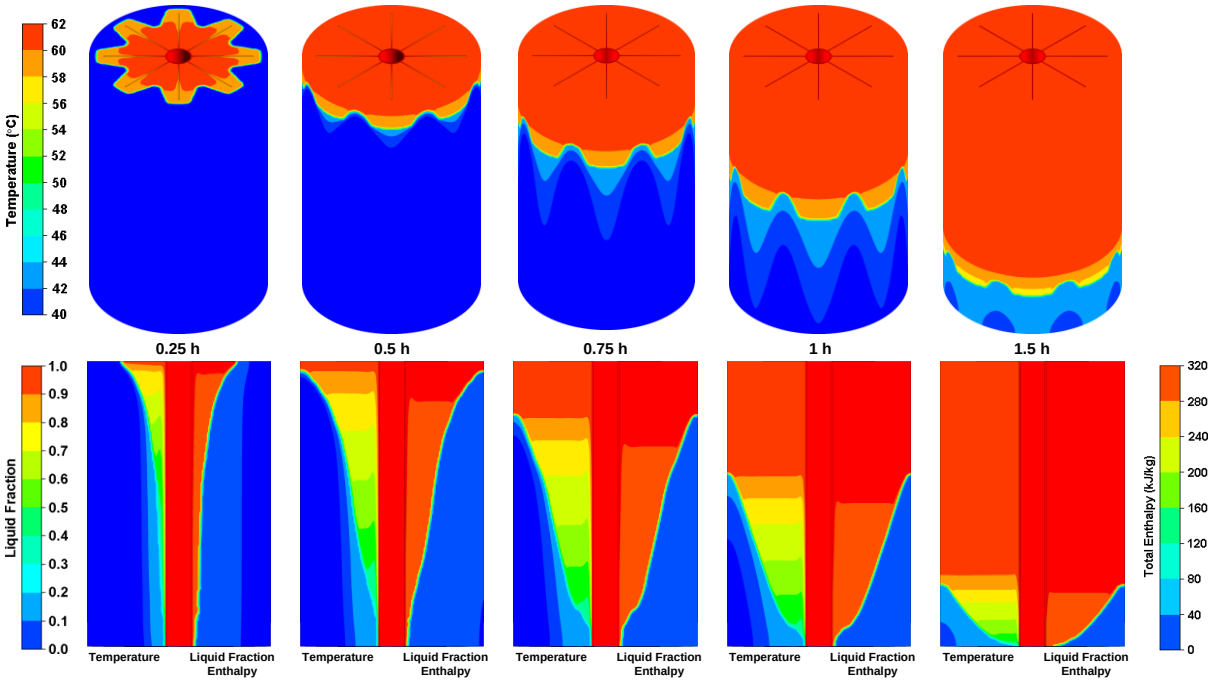
Temperature (°C)
62
60
58
56
54
52
50
48
46
44
42
40
0.25 h
0.5 h
0.75 h
1 h
1.5 h
Liquid Fraction
1.0
0.9
0.8
0.7
0.6
0.5
0.4
0.3
0.2
0.1
0.0
Temperature
Liquid Fraction
Enthalpy
Total Enthalpy (kJ/kg)
320
280
240
200
160
120
80
40
0

(b)

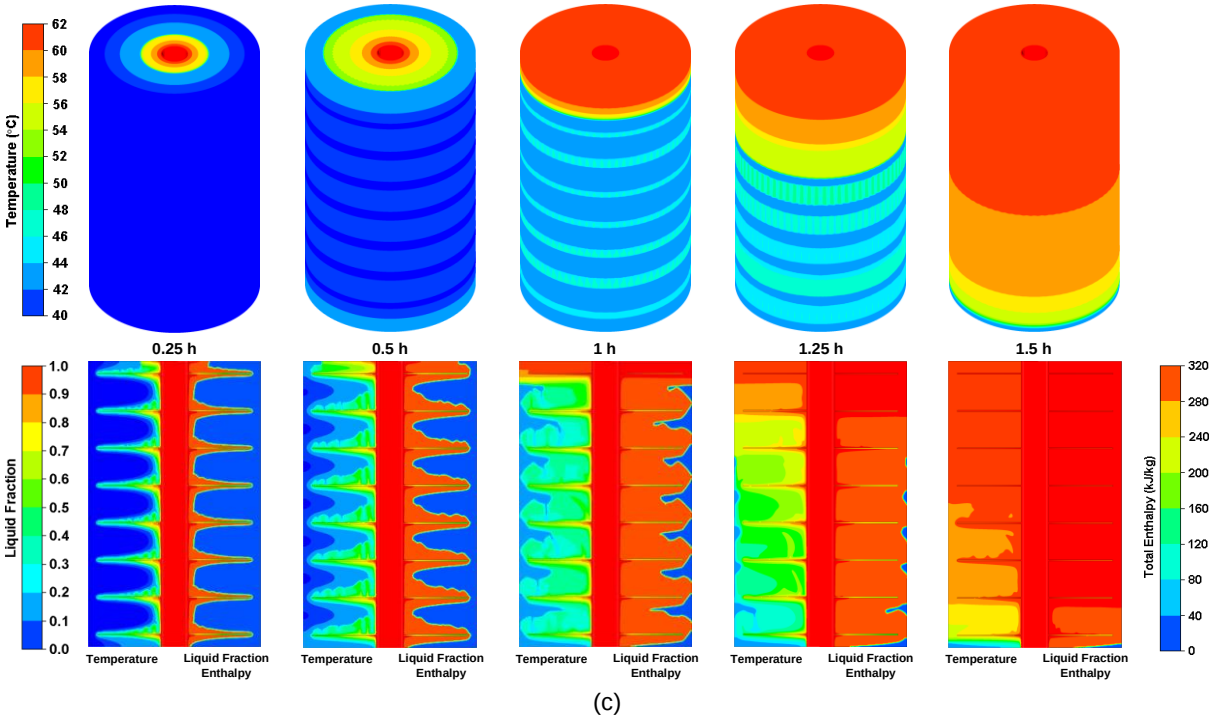

(c)

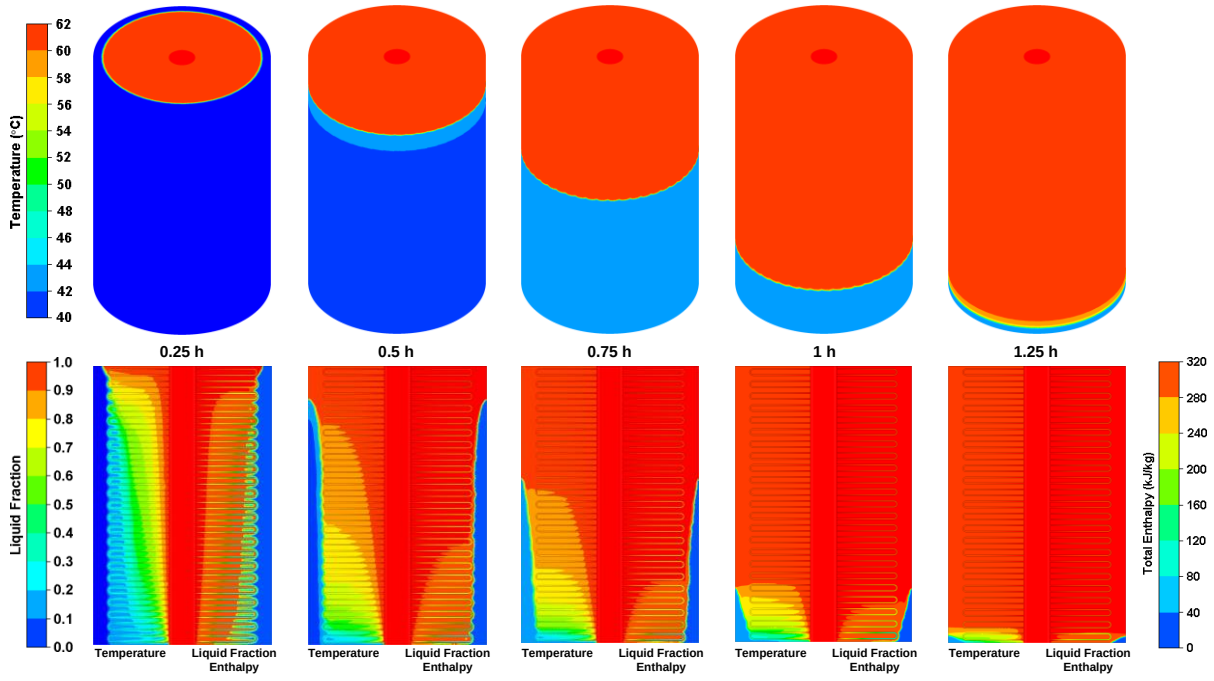

(d)

Fig. 5 Temperature, liquid fraction and enthalpy contours of (a) nano-PCM in shell-and-tube without extended surfaces (case 2), (b) paraffin in shell-and-tube with longitudinal fins (case 3), (c) paraffin in shell-and-tube with circular fins (case 7) and (d) paraffin in shell-and-tube with wire-wound fins (case 11) while charging at constant inlet temperature of 62 ^{o}C.

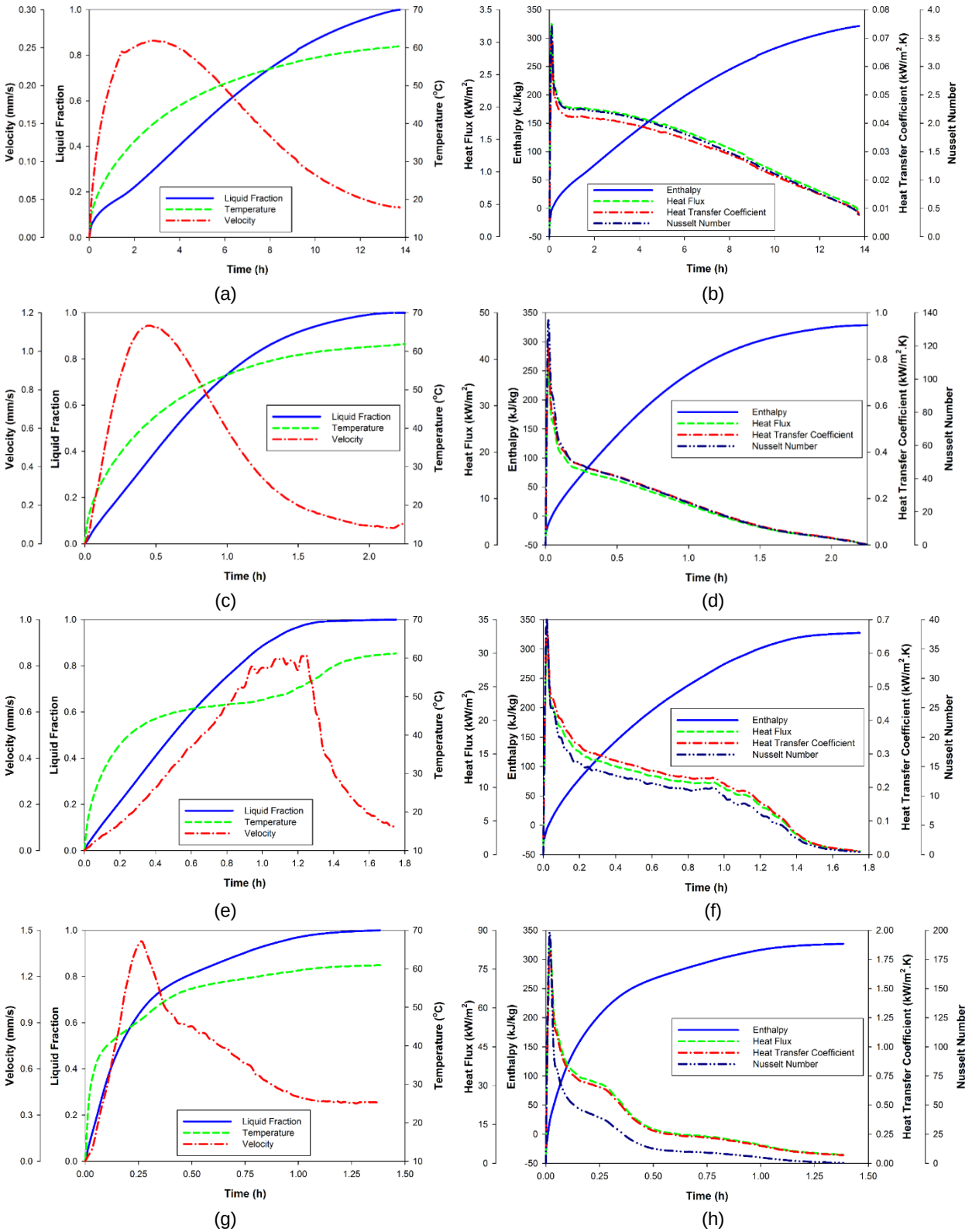

438 **Fig. 6** Transient behaviour of (a-b) nano-PCM in shell-and-tube without extended surfaces (case 2),
439 (c-d) paraffin in shell-and-tube with longitudinal fins (case 3), (e-f) paraffin in shell-and-tube with
440 circular fins (case 7) and (g-h) paraffin in shell-and-tube with wire-wound fins (case 11) during the
441 course of charging cycle.

3.6. Coupled heat transfer enhancement

In this section, the influence of coupled thermal performance enhancement with three volume concentrations of graphene nano-platelets and extended surfaces are analysed and compared to identify an optimal design solution for LHS systems. As listed in **Table 2**, the nano-PCMs with longitudinal fins in case 4–6, with circular fins in case 8–10 and with wire-wound fins in case 12–14 are evaluated by numerical simulations of charging cycles. The nano-PCMs with three varied volume concentrations i.e. 1%, 3% and 5% and their respective packing factors of 0.965, 0.945 and 0.925 are investigated.

Temperature, enthalpy and liquid fraction contours for coupled enhancement scenarios, while charging at constant inlet temperature of 62 ^{o}C for 0.5 h, are illustrated in **Fig. 7**. Similarly, the transient responses of liquid fraction and heat flux to charging cycles are illustrated in **Fig. 8**. The effective thermal conductivity of nano-PCMs are augmented with inclusion of graphene nano-platelets. As a result, the heat fluxes for all scenarios in conduction dominant earlier stages are improved with increasing volume concentrations. For instance, the maximum heat fluxes for longitudinal fins are increased from 39 kW/m^2 for paraffin to 47.23 kW/m^2, 47.26 kW/m^2 and 47.69 kW/m^2 for nano-PCMs with 1%, 3% and 5% volume concentrations, respectively. Likewise, the peak heat fluxes for circular and wire-wound fins are observed to increase from 31.11 kW/m^2 to 35.86, 35.90, 35.97 kW/m^2 and from 82.93 kW/m^2 to 88.13, 88.74 and 89.21 kW/m^2, respectively. In consequence, the thermal energy in conduction dominant earlier stages are rapidly captured.

In subsequent stages, the buoyancy driven natural convection influences the upward rise of liquid nano-PCMs. However, the impacts of natural convection on thermal propagations and charging rates are compromised by augmented dynamic viscosity of nano-PCMs. Due to which, the overall heat flux, mean velocity and Nu for nano-PCMs with increasing volume concentrations have registered decreasing trends for all extended surfaces. For instance, in case of longitudinal fins, the peak values for mean velocity and Nu for nano-PCMs are decreased from 1.48 mm/s to 1.33 mm/s and 93.20 to 88.35 with an increase in volume concentration from 1% to 5%, respectively. In case of circular fins, the peak values for mean velocity and Nu for nano-PCMs are reduced from 0.96 mm/s to 0.70 mm/s and 28.33 to 26.71, respectively. Likewise, in case of wire-wound fins, the peak values for mean velocity and Nu for nano-PCMs are declined from 1.64 mm/s to 1.40 mm/s and 144.30 to 132.80, respectively. Hence, the predominant augmentation in dynamic viscosity with increasing volume concentrations can overweight the enhancement in effective thermal conductivity and can potentially decelerate the melting process in these later stages of charging cycle. Similar findings from both numerical and experimental studies are reported in previous literature [49-52].

In spite of weaker natural convection, the overall heat fluxes for nano-PCMs are relatively higher as compared to paraffin without nano-additives, as presented in **Fig. 8**. In final stages, the complexities of liquid congestions and weaker mobility are subdued by higher heat fluxes of nano-PCMs, which results in rapid transport of thermal energy to bottom region of shell container.

Hence, the overall charging times for coupled enhancement scenarios are significantly reduced, as presented in **Fig. 9**. In comparison to paraffin in plain tube configuration (case 1), the total charging times for nano-PCMs with 1% graphene nano-platelets in longitudinal,

circular and wire-wound fins configurations are significantly reduced by 94.17%, 94.87% and 96.08%, respectively. Likewise, by substituting paraffin with nano-PCMs with 1% graphene nano-platelets, the total charging durations for longitudinal, circular and wire-wound fins configurations can be further reduced by 32.44%, 24% and 26.09%, respectively. However, with an increase in volume concentrations, the overall charging durations have either remained similar for circular and wire-wound fins configurations or have increased for longitudinal fins configuration, as shown in **Fig. 9**. Similarly, the temperature and enthalpy contours of nano-PCMs in longitudinal, circular and wire-wound fins configurations have demonstrated insignificant variations with increasing volume concentrations, as illustrated in **Fig. 7**. The reasons behind are the disadvantages associated with increasing dynamic viscosity in terms of weakened thermal propagation and natural convection.

As provided in **Table 2**, the packing factor values decrease with inclusion of extended surfaces and nano-additives. In consequence, the total volume available for pure paraffin in shell container is compromise. Therefore, the total enthalpy for paraffin with extended surfaces configurations are reduced to 11.28 MJ as compared to 11.52 MJ for paraffin in plain tube configuration (case 1). Similarly, the total enthalpy for extended surfaces are further reduced by inclusion of graphene nano-platelets with 1%, 3% and 5% volume concentrations to 11.09 MJ, 10.72 MJ and 10.38 MJ, respectively.

Moreover, the potential costs associated with inclusion of graphene nano-platelets is another fundamental factor in establishing the optimal volume concentration [53]. **Table 5** provides the cost estimations for paraffin and nano-PCMs with varied volume concentrations for shell-and-tube with extended surfaces configurations (case 3 – 14). As compared to paraffin, the total price for nano-PCMs with 1%, 3% and 5% volume concentrations are increased by 21.84%, 71.85% and 123.97%, respectively. Hence, in addition to increasing dynamic viscosity and reducing total enthalpy, the significant increase in total price of nano-PCMs persuade to recommend nano-PCMs with 1% volume concentration.

To conclude, the coupled enhancement scenarios have significantly shortened the overall charging duration at minimal expense of total enthalpy. Amongst the three extended surfaces configurations, the novel design of wire-wound fins configuration has demonstrated relatively higher charging rates, higher heat fluxes and better thermal distributions for both paraffin and nano-PCM. Therefore, the wire-wound fins configurations with paraffin in case 11 and with nano-PCM in case 12 are recommended for utilisation in large-scale domestic and commercial applications.

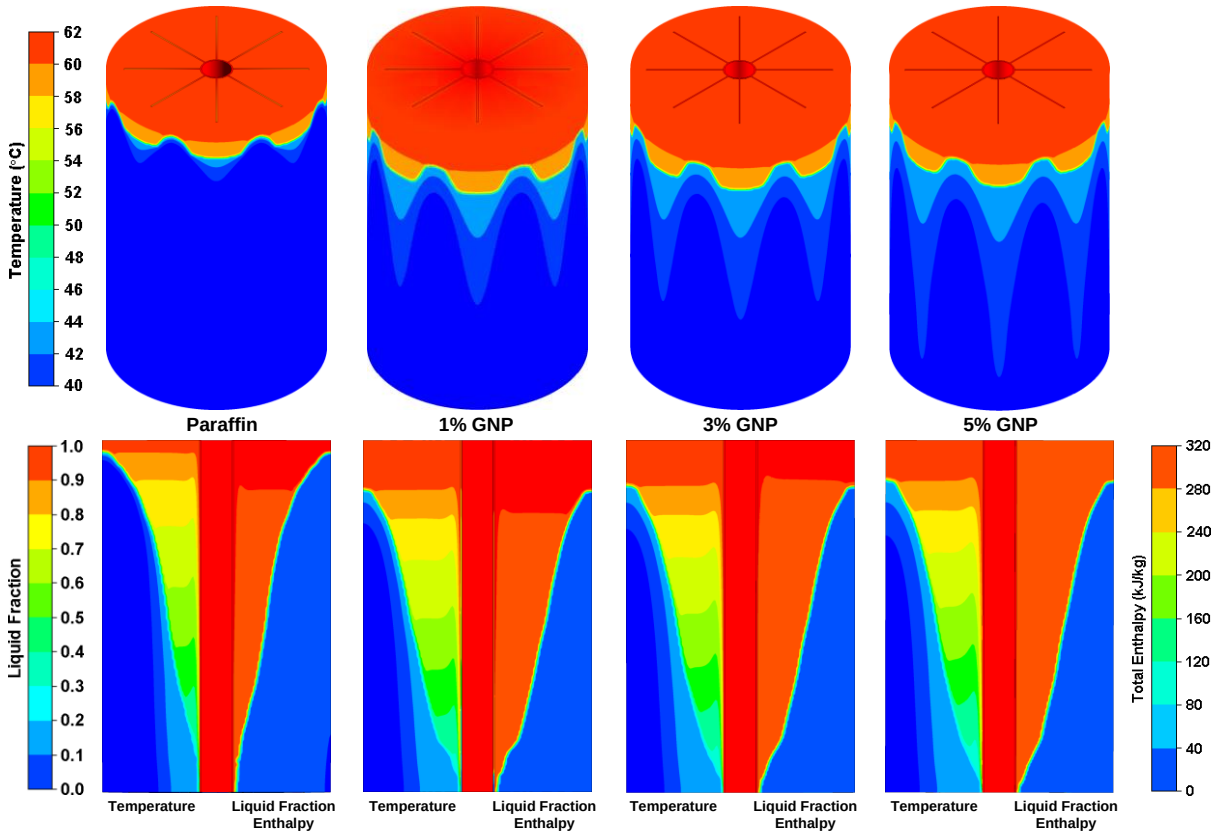
Temperature (°C)
62
60
58
56
54
52
50
48
46
44
42
40
Paraffin
1% GNP
3% GNP
5% GNP
Liquid Fraction
1.0
0.9
0.8
0.7
0.6
0.5
0.4
0.3
0.2
0.1
0.0
Temperature
Liquid Fraction
Enthalpy
Total Enthalpy (kJ/kg)
320
280
240
200
160
120
80
40
0

(a)

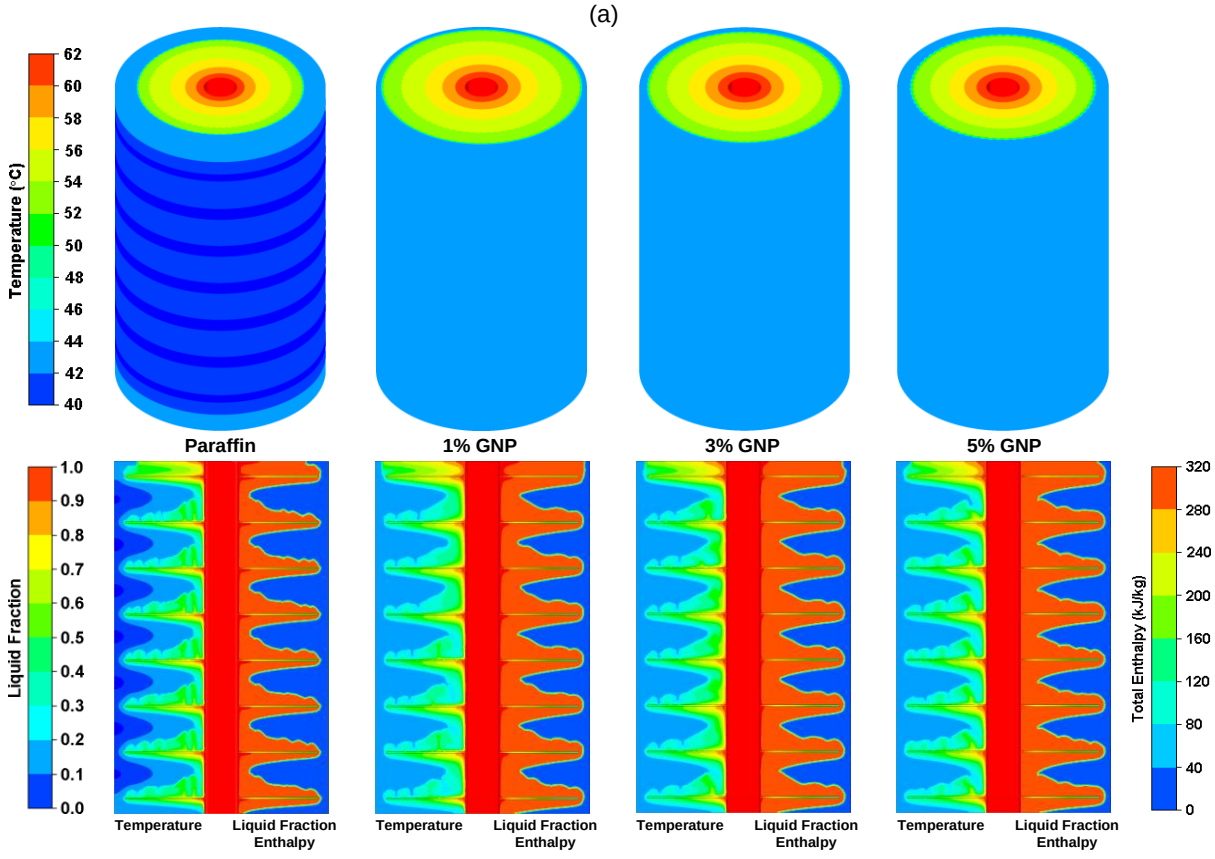
Temperature (°C)
62
60
58
56
54
52
50
48
46
44
42
40
Paraffin
1% GNP
3% GNP
5% GNP
Liquid Fraction
1.0
0.9
0.8
0.7
0.6
0.5
0.4
0.3
0.2
0.1
0.0
Temperature
Liquid Fraction
Enthalpy
Total Enthalpy (kJ/kg)
320
280
240
200
160
120
80
40
0

(b)

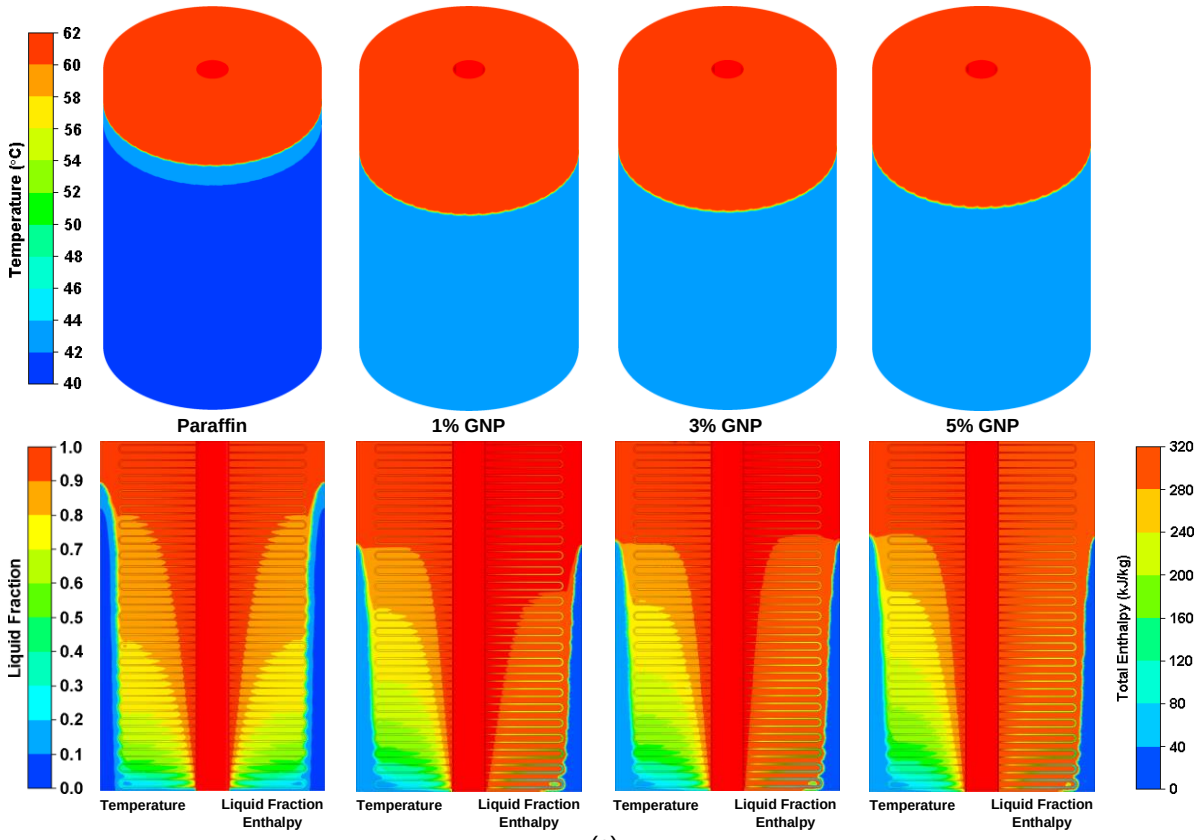

(c)

Fig. 7 Temperature contours, liquid fractions and enthalpy behaviour of paraffin and nano-PCMs with three varied volume concentrations in (a) longitudinal, (b) circular and (c) wire-wound fins configurations while charging for 0.5 h at constant inlet temperature of 62 ^{o}C.

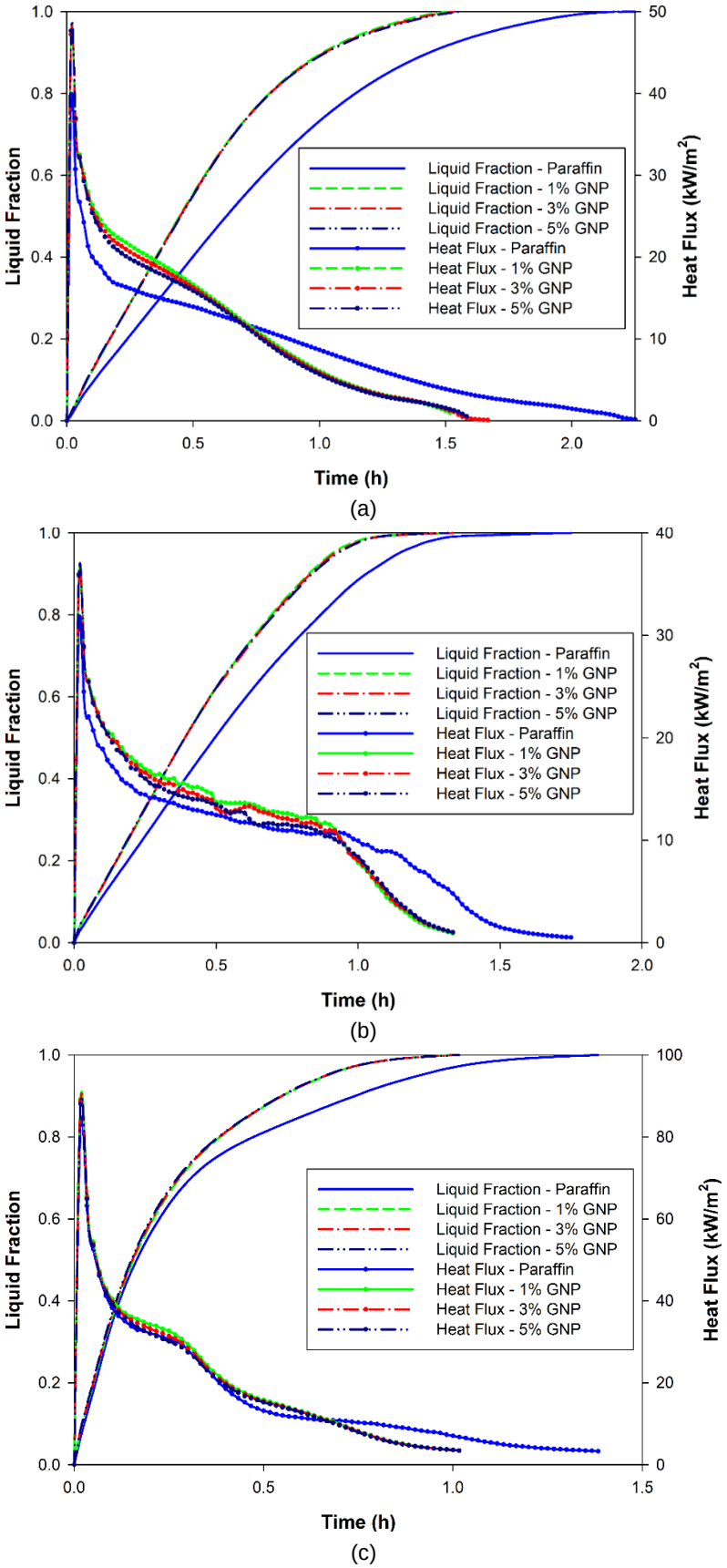

523 **Fig. 8** Liquid fraction and heat flux response to charging cycles of paraffin and nano-PCMs with three
524 varied volume concentrations in: (a) longitudinal, (b) circular and (c) wire-wound fins configurations.

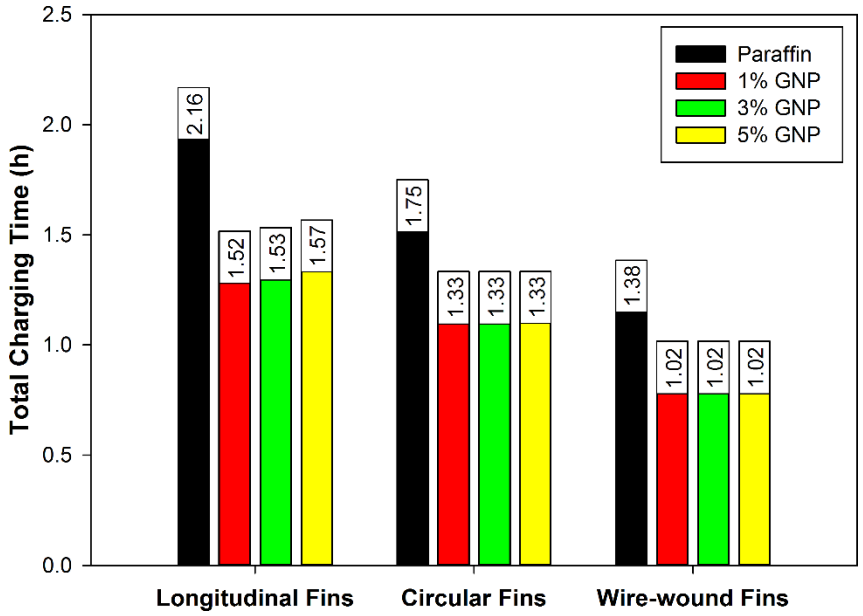

Fig. 9 Total charging duration of paraffin and nano-PCMs with varied volume concentrations in longitudinal, circular and wire-wound fins configurations.

Table 5
Cost evaluation for nano-PCMs with varied volume concentrations

PCM in extended surfaces configurations	Weight of paraffin (kg)	Price of paraffin (€) *	Weight of GNP (kg) ***	Price of GNP (€) **	Total price of nano-PCM (€)	Percentage increase (%)
Paraffin	35.21	502.05	-	-	502.05	-
Nano-PCM with 1% GNP	34.01	484.98	0.20	126.72	611.70	21.84
Nano-PCM with 3% GNP	33.29	474.77	0.61	387.99	862.77	71.85
Nano-PCM with 5% GNP	32.55	464.14	1.03	660.27	1124.41	123.97

* Price of paraffin (RT44HC) = 14.26 €/kg [40]

** Price of GNP = 639.00 €/kg [41]

*** $w_{NP} = \left(\frac{\Phi_{VC}}{100-\Phi_{VC}}\right)(\rho_{NP} V_{NPCM})$

4. Conclusions

This article is focused on 3-dimensional transient numerical simulations of coupled thermal performance enhancement by including graphene based nano-PCMs and three extended surfaces based shell-and-tube configurations for LHS applications. The extended surfaces include longitudinal, circular and wire-wound fins and the varied volume concentrations of graphene nano-platelets are chosen as 1%, 3% and 5%. In total, fourteen coupled enhancement cases are investigated to identify the optimal thermal performance scenario with higher charging rate, total enthalpy and better thermal distribution in shell container. Based on numerical simulation of charging cycles, the following conclusions are derived:

- Thermal distributions and phase transition rates of paraffin for extended surfaces are relatively higher as compared to graphene based nano-PCMs. Moreover, the heat fluxes, heat transfer coefficients and Nu for extended surfaces are higher due their extended thermal reach and higher heat transfer area as compared to nano-PCMs. For instance, the total charging duration is reduced from 26 h for pure paraffin in shell-and-tube without extended surfaces (case 1) to 13.75 h for graphene nano-platelets

enhanced paraffin in shell-and-tube without extended surfaces (case 2). Whereas, the total charging duration for paraffin is significantly shortened to 2.16 h, 1.75 h and 1.38 h for longitudinal (case 3), circular (case 7) and wire-wound (case 11) fins.

- Natural convection is crucial for melt front propagation, thermal distribution and charging rate of LHS system. It is noticed that with inclusion of graphene nano-platelets, the effective thermal conductivity and dynamic viscosity of paraffin are significantly improved. Hence, the influence of increment in thermal conductivity on buoyancy driven natural convection is moderated with escalation in dynamic viscosity. Likewise, the geometrical orientations of extended surfaces are significantly influential for thermal distribution and melt front propagation. For instance, the circular fins orientation restricts the upward rise of liquefied paraffin, whereas the longitudinal and wire-wound fins orientations supplements the buoyancy driven upward movement. Hence, the Nu for circular fins orientation peaks to 39.32, whereas it peaks to 131.8 and 197.2 for longitudinal and wire-wound fins configurations.
- Thermal performance of extended surfaces are further enhanced with nano-PCMs. Heat fluxes and charging rates are significantly improved with inclusion of 1% volume concentration of graphene nano-platelets. For instance, the heat fluxes are increased from 39 – 47.23 kW/m^2 for longitudinal fins, 31.11 – 35.86 kW/m^2 for circular fins and 82.93 – 88.13 kW/m^2 for wire-wound fins configurations. In consequence, the total charging durations are further reduced from 2.16 – 1.52 h, 1.75 – 1.33 h and 1.38 – 1.02 h for longitudinal, circular and wire-wound fins configurations, respectively.
- Higher volume concentrations have adverse impacts on total enthalpy, natural convection and melt front propagation. Total enthalpy is reduced from 11.28 MJ for paraffin with extended surfaces to 10.38 MJ for nano-PCM with 5% volume concentration. Likewise, due to weaker natural convection with increasing dynamic viscosity, the overall charging durations are either similar or increased with increasing volume concentrations from 1% to 5%. In order to acquire higher charging rates at minimal expense of total enthalpy and economic cost, the nano-PCM with 1% volume concentration is recommended for shell-and-tube with extended surfaces.
- The novel design of wire-wound fins configuration has illustrated relatively higher charging rate, better thermal distribution and insignificant reduction in total enthalpy. In case of pure paraffin in wire-wound fins configuration (case 11), the total enthalpy of 11.28 MJ is captured in mere 1.38 h as compared to 24.5 h for paraffin in shell-and-tube without extended surfaces (case 1). In order to compare with other extended surfaces, the charging rate for equal amount of thermal enthalpy (11.28 MJ) in wire-wound fins configuration is 35.96% and 20.95% higher than longitudinal and circular fins configurations. Moreover, the coupled thermal enhancement with nano-PCM in wire-wound fins configuration has presented significantly higher charging performance of capturing 11.09 MJ in as little as 1.02 h. Hence, the coupled enhancement scenario of wire-wound fins configuration with both paraffin and nano-PCM are recommended for wider practical applications. This proposed design LHS system with its longer service life, minimal maintenance and adaptable scalability will bring significant enhancements to energy security, energy system efficiencies and reliabilities.

Acknowledgement

Authors would like to acknowledge Bournemouth University, UK for funding this research.

References

[1] IEA. Energy and Climate Change International Energy Agency (IEA), 21st UN Conference of the Parties (COP21), Paris, 2015.

[2] REN21. Renewables 2019 Global Status Report, Paris: REN21 Secretariat, 2019.

[3] B. Dudley. BP Statistical Review of World Energy. 68th ed, London, 2019.

[4] J.P. da Cunha, P. Eames. Thermal energy storage for low and medium temperature applications using phase change materials–a review. Applied Energy. 177 (2016) 227-38.

[5] Z. Khan, Z. Khan, A. Ghafoor. A review of performance enhancement of PCM based latent heat storage system within the context of materials, thermal stability and compatibility. Energy Conversion and Management. 115 (2016) 132-58.

[6] A.M. Abdulateef, S. Mat, J. Abdulateef, K. Sopian, A.A. Al-Abidi. Geometric and design parameters of fins employed for enhancing thermal energy storage systems: a review. Renewable and Sustainable Energy Reviews. 82 (2018) 1620-35.

[7] M. Al-Maghalseh, K. Mahkamov. Methods of heat transfer intensification in PCM thermal storage systems. Renewable and Sustainable Energy Reviews. 92 (2018) 62-94.

[8] J.M. Mahdi, S. Lohrasbi, E.C. Nsofor. Hybrid heat transfer enhancement for latent-heat thermal energy storage systems: A review. International Journal of Heat and Mass Transfer. 137 (2019) 630-49.

[9] H. Niyas, S. Prasad, P. Muthukumar. Performance investigation of a lab–scale latent heat storage prototype–Numerical results. Energy Conversion and Management. 135 (2017) 188-99.

[10] M.M. Joybari, F. Haghighat, S. Seddegh, A.A. Al-Abidi. Heat transfer enhancement of phase change materials by fins under simultaneous charging and discharging. Energy Conversion and Management. 152 (2017) 136-56.

[11] Z. Khan, Z. Khan, K. Tabeshf. Parametric investigations to enhance thermal performance of paraffin through a novel geometrical configuration of shell and tube latent thermal storage system. Energy Conversion and Management. 127 (2016) 355-65.

[12] Z. Khan, Z.A. Khan. An experimental investigation of discharge/solidification cycle of paraffin in novel shell and tube with longitudinal fins based latent heat storage system. Energy Conversion and Management. 154 (2017) 157-67.

[13] Z. Khan, Z.A. Khan. Experimental investigations of charging/melting cycles of paraffin in a novel shell and tube with longitudinal fins based heat storage design solution for domestic and industrial applications. Applied Energy. 206 (2017) 1158-68.

[14] S. Tiari, S. Qiu. Three-dimensional simulation of high temperature latent heat thermal energy storage system assisted by finned heat pipes. Energy Conversion and Management. 105 (2015) 260-71.

[15] X. Yang, Z. Lu, Q. Bai, Q. Zhang, L. Jin, J. Yan. Thermal performance of a shell-and-tube latent heat thermal energy storage unit: Role of annular fins. Applied energy. 202 (2017) 558-70.

[16] S. Lohrasbi, M. Gorji-Bandpy, D.D. Ganji. Thermal penetration depth enhancement in latent heat thermal energy storage system in the presence of heat pipe based on both charging and discharging processes. Energy Conversion and Management. 148 (2017) 646-67.

[17] A. Caron-Soupart, J.-F. Fourmigué, P. Marty, R. Couturier. Performance analysis of thermal energy storage systems using phase change material. Applied Thermal Engineering. 98 (2016) 1286-96.

[18] A. Rozenfeld, Y. Kozak, T. Rozenfeld, G. Ziskind. Experimental demonstration, modeling and analysis of a novel latent-heat thermal energy storage unit with a helical fin. International Journal of Heat and Mass Transfer. 110 (2017) 692-709.

[19] S. Borhani, M. Hosseini, A. Ranjbar, R. Bahrampoury. Investigation of phase change in a spiral-fin heat exchanger. Applied Mathematical Modelling. 67 (2019) 297-314.

[20] J. Vogel, M. Johnson. Natural convection during melting in vertical finned tube latent thermal energy storage systems. Applied Energy. 246 (2019) 38-52.

[21] A. Pizzolato, A. Sharma, K. Maute, A. Sciacovelli, V. Verda. Design of effective fins for fast PCM melting and solidification in shell-and-tube latent heat thermal energy storage through topology optimization. Applied energy. 208 (2017) 210-27.

[22] M.E.H. Amagour, A. Rachek, M. Bennajah, M.E. Touhami. Experimental investigation and comparative performance analysis of a compact finned-tube heat exchanger uniformly filled with a phase change material for thermal energy storage. Energy conversion and management. 165 (2018) 137-51.

[23] D. Li, C. Yang, H. Yang. Experimental and numerical study of a tube-fin cool storage heat exchanger. Applied Thermal Engineering. 149 (2019) 712-22.

[24] H.M. Ali, M.J. Ashraf, A. Giovannelli, M. Irfan, T.B. Irshad, H.M. Hamid, et al. Thermal management of electronics: an experimental analysis of triangular, rectangular and circular pin-fin heat sinks for various PCMs. International Journal of Heat and Mass Transfer. 123 (2018) 272-84.

[25] A. Arshad, H.M. Ali, S. Khushnood, M. Jabbal. Experimental investigation of PCM based round pin-fin heat sinks for thermal management of electronics: effect of pin-fin diameter. International Journal of Heat and Mass Transfer. 117 (2018) 861-72.

[26] Z. Khan, Z.A. Khan. Thermodynamic performance of a novel shell-and-tube heat exchanger incorporating paraffin as thermal storage solution for domestic and commercial applications. Applied Thermal Engineering. (2019) 114007.

[27] M. Said, H. Hassan. Effect of using nanoparticles on the performance of thermal energy storage of phase change material coupled with air-conditioning unit. Energy conversion and management. 171 (2018) 903-16.

[28] S. Ebadi, S.H. Tasnim, A.A. Aliabadi, S. Mahmud. Melting of nano-PCM inside a cylindrical thermal energy storage system: Numerical study with experimental verification. Energy conversion and management. 166 (2018) 241-59.

[29] S.I. Golestaneh, G. Karimi, A. Babapoor, F. Torabi. Thermal performance of co-electrospun fatty acid nanofiber composites in the presence of nanoparticles. Applied energy. 212 (2018) 552-64.

[30] Z. Khan, Z.A. Khan. Experimental and numerical investigations of nano-additives enhanced paraffin in a shell-and-tube heat exchanger: A comparative study. Applied Thermal Engineering. 143 (2018) 777-90.

[31] R.J. Warzoha, A.S. Fleischer. Improved heat recovery from paraffin-based phase change materials due to the presence of percolating graphene networks. International Journal of Heat and Mass Transfer. 79 (2014) 314-23.

[32] Y. Tang, D. Su, X. Huang, G. Alva, L. Liu, G. Fang. Synthesis and thermal properties of the MA/HDPE composites with nano-additives as form-stable PCM with improved thermal conductivity. Applied energy. 180 (2016) 116-29.

[33] Y. Yuan, N. Zhang, T. Li, X. Cao, W. Long. Thermal performance enhancement of palmitic-stearic acid by adding graphene nanoplatelets and expanded graphite for thermal energy storage: A comparative study. Energy. 97 (2016) 488-97.

[34] Z.-T. Yu, X. Fang, L.-W. Fan, X. Wang, Y.-Q. Xiao, Y. Zeng, et al. Increased thermal conductivity of liquid paraffin-based suspensions in the presence of carbon nano-additives of various sizes and shapes. Carbon. 53 (2013) 277-85.

[35] J.M. Mahdi, E.C. Nsofor. Solidification enhancement of PCM in a triplex-tube thermal energy storage system with nanoparticles and fins. Applied energy. 211 (2018) 975-86.

[36] R.P. Singh, S. Kaushik, D. Rakshit. Melting phenomenon in a finned thermal storage system with graphene nano-plates for medium temperature applications. Energy conversion and management. 163 (2018) 86-99.

[37] R.P. Singh, S. Kaushik, D. Rakshit. Solidification behavior of binary eutectic phase change material in a vertical finned thermal storage system dispersed with graphene nano-plates. Energy conversion and management. 171 (2018) 825-38.

[38] M. Sheikholeslami, R.-u. Haq, A. Shafee, Z. Li, Y.G. Elaraki, I. Tlili. Heat transfer simulation of heat storage unit with nanoparticles and fins through a heat exchanger. International Journal of Heat and Mass Transfer. 135 (2019) 470-8.

[39] M. Parsazadeh, X. Duan. Numerical study on the effects of fins and nanoparticles in a shell and tube phase change thermal energy storage unit. Applied energy. 216 (2018) 142-56.

[40] Rubitherm® Technologies GmbH, http://www.rubitherm.eu/en/. 2019.

[41] Iolitec Ionic Liquids Technologies GmbH, https://iolitec.de/en. 2019.

[42] D.D. Gray, A. Giorgini. The validity of the Boussinesq approximation for liquids and gases. International Journal of Heat and Mass Transfer. 19 (1976) 545-51.

[43] D.A. Nield, A. Bejan, Nield-Bejan... Convection in porous media. Springer2006.

[44] J.M. Mahdi, S. Lohrasbi, D.D. Ganji, E.C. Nsofor. Accelerated melting of PCM in energy storage systems via novel configuration of fins in the triplex-tube heat exchanger. International Journal of Heat and Mass Transfer. 124 (2018) 663-76.

[45] M. Corcione. Empirical correlating equations for predicting the effective thermal conductivity and dynamic viscosity of nanofluids. Energy Conversion and Management. 52 (2011) 789-93.

[46] R. Kandasamy, X.-Q. Wang, A.S. Mujumdar. Transient cooling of electronics using phase change material (PCM)-based heat sinks. Applied Thermal Engineering. 28 (2008) 1047-57.

[47] R.S. Vajjha, D.K. Das. Experimental determination of thermal conductivity of three nanofluids and development of new correlations. International Journal of Heat and Mass Transfer. 52 (2009) 4675-82.

[48] S. Deng, C. Nie, H. Jiang, W.-B. Ye. Evaluation and optimization of thermal performance for a finned double tube latent heat thermal energy storage. International Journal of Heat and Mass Transfer. 130 (2019) 532-44.

[49] L.-W. Fan, Z.-Q. Zhu, Y. Zeng, Q. Lu, Z.-T.J.I.J.o.H. Yu, M. Transfer. Heat transfer during melting of graphene-based composite phase change materials heated from below. 79 (2014) 94-104.

[50] Y. Zeng, L.-W. Fan, Y.-Q. Xiao, Z.-T. Yu, K.-F.J.I.J.o.H. Cen, M. Transfer. An experimental investigation of melting of nanoparticle-enhanced phase change materials (NePCMs) in a bottom-heated vertical cylindrical cavity. 66 (2013) 111-7.

[51] M. Parsazadeh, X.J.A.E. Duan. Numerical study on the effects of fins and nanoparticles in a shell and tube phase change thermal energy storage unit. 216 (2018) 142-56.

[52] D. Zou, X. Ma, X. Liu, P. Zheng, Y.J.I.J.o.H. Hu, M. Transfer. Thermal performance enhancement of composite phase change materials (PCM) using graphene and carbon nanotubes as additives for the potential application in lithium-ion power battery. 120 (2018) 33-41.

[53] Z. Khan, Z.A. Khan, P. Sewell. Heat transfer evaluation of metal oxides based nano-PCMs for latent heat storage system application. 144 (2019) 118619.